tmp title: MUSC source

Damien Pageot[*†], **Donatienne Leparoux**[*], **Mathieu Le Feuvre**[*], **Olivier Durand**[*] **and Yann Capdeville**[‡]

[*]*LUNAM-IFSTTAR,*

[†]*OSUNA*

[*]*LPGN,*

(October 27, 2015)

ABSTRACT

INTRODUCTION

Since the early developments of seismic imaging methods in the middle of 20th century, approaches and algorithms innovations are still proposed in current research projects. The improvements deal with both the qualitative imaging techniques like migration (e.g. Berkhout et al. (2012); Guofeng et al. (2013)), novel applications of quantitative imaging methods such as the first arrival tomography (e.g. Bohm et al. (2015)), or even more recent approaches like the Full Waveform Inversion (e.g. Perez Solano et al. (2014), see Virieux and Operto (2009) for a revue of this last decade). The refinements are proposed for different scales like near surface applications for civil engineering topics or more deeper investigation for example for oil prospection or crustal imaging at regional or global scales. They are mostly validated by using synthetic data, for example with well known shared benchmark (like the Marmousi case). However, the synthetic data are generally computed using the same wave propagation modeling engine used in the inverse problem process. In other terms, the synthetic data are computed with some assumptions which are the same in the inverse problem, for example the approximation of acoustic propagation, a 2D space medium, or a 2D line source. This approach, called *inverse crime* (Wirgin, 2004) is particularly useful for validating an algorithm in its early development stage but does not take into account the artefacts that can be due to the assumptions of the direct problem. Some authors tackle this issue by providing 3D data which are inverted with a 2D approach or other restrictive assumptions (e.g). But also in this case, the approach does not allow to assess the efficiency of the method for real seismic data. Moreover, because no one knows precisely the Earth interior, it is difficult to evaluate the capacity of a method to recover physical parameters and structures from real seismic data which can lead sometimes to geological misinterpretation due to numerical artifacts (Morozov, 2004). Thus, it is necessary to add

a step for which imaging methods will be tested for experimental seismic measurements obtained under controlled conditions.

The best way to satisfy this need is to use Physical Small Scale Modeling Methods (noted *PSM* subsequently). *PSM* were used since several years to study the propagation of waves in various media with several stage of complexity, from acoustic wave propagation in homogeneous media to elastic wave propagation in three-dimensional heterogeneous anisotropic media (Rieber, 1936; Howes et al., 1953; Hilterman, 1970; French, 1974; Bishop et al., 1985; Pratt, 1999; Favretto-Cristini et al., 2013; Sarkar et al., 2003; Isaac and Lawton, 1999), and allow to generate experimental seismic data under well-controlled conditions. In this way, recent studies have been conducted to simulate multi-sources and multi-receivers through piezo-electric transducers (Wong et al., 2009). An alternative approach consists in using the laser interferometry as the receiver system, as done in the MUSC Laboratory (Bretaudeau et al., 2008, 2011, 2013), *Mesure Ultrasonore Sans Contact* in French, is one of them. This technology, by avoiding the contact of the receivers on the model, allows to by-pass the coupling issue of transducers that is difficult to model. In this way,the MUSC laboratory is designed to simulate (1) wide-angle on-shore acquisitions modeling both body waves and surface waves, (2) automatic multisource-multireceiver measurements with a high-productivity, (3) high-precision source-receiver positioning and (4) high-precision recording of absolute surface displacement without coupling effects.

Our objective here is to increase the potential of the MUSC system as a reliable tool for generating experimental data which will be distributed in the scientific community. Thus, we present two studies of experimental data in order to : 1) quantitatively refine the comparison between numerical and experimental data by taking into account the 3D/2D geometrical spreading effects through an alternative way and 2) identify the reproducibility

3

of the source impact and, consequently, data repeatability. These approaches will complete the knowledge of the system and facilitate the achievement of massive multi-source and multi-receiver data simulating subsurface seismic experimental campaigns. Moreover, they provide quantitative informations about the data quality for geophysicists who need to use them measurement based on reduced scale model.

In order to achieve these objectives, we used a seismic wave modeling code based on the Spectral Element Method (Komatitsch et al., 1998; Komatitsch and Tromp, 1999; Komatitsch et al., 2005; Festa and Vilotte, 2005) that allow to provide numerical signals as reference data for comparison. The Spectral Element Method (SEM) has several advantages compared to finite differences and finite elements, such as: (1) a weak formulation which can naturally take into account the free surface, (2) an explicit scheme in time domain facilitating parallelization and reducing the computational cost, (3) a spatial discretization (mesh) convenient for the representation of complex environments and (4) high precision results and low numerical dispersion.

The numerical characteristics of the code used are described in a first part below. Afterwards, the specificities of the MUSC system are explained, followed by the presentation of the models used. Finally The two coupled studies on experimental data are detailed, in the respective aims (1) of refining the comparison between numerical and experimental data by taking into account the geometrical spreading effects between two-dimensional and three-dimensional data through an alternative way, and (2) of identifying the reproducibility of the source impact to validate the data reproducibility.

METHODS

Numerical modeling: Spectral Element Method

Various numerical methods exist to resolve the equation of motion in arbitrary elastic media. The most widely used for seismic applications is the Finite-Differences (FD) method (Virieux, 1986; Levander, 1988; Robertsson et al., 1994; Pratt, 1990; Stekl and Pratt, 1998; Saenger and Bohlen, 2004) which estimates each derivative on a regular Cartesian grid using a Taylor development (Moczo et al., 2004) of order n. FD is simple to implement and robust but quickly shows some limitations. First the Cartesian grid is defined by the minimum propagated wavelength (λ_{min}) in the full medium which conducts to a very small spatial step in case of low velocities zones it is usually the case for subsurface issues. Moreover, Saenger et al. (2000) show that 60 points by wavelength (λ) are needed to model propagation of Rayleigh wave in order $n = 2$ where only 15 points by λ are required to model propagation of body waves which increases drastically the numerical cost in case of near-surface modeling experiment. Second, the Cartesian grid does not provide a suitable tool to reproduce properly complex topography and interfaces.

To overcome this limit, one can use the Finite-Elements Method (FEM) which is another popular method used for wave propagation modeling (Lysmer and Drake, 1972; Seron et al., 1990; Hulbert and Hughes, 1990). FEM is based on a variational formulation of the equation of motion and gives a continuous approximate solution in space using polynomial basis functions defined on each node of each cell of the mesh. The natural boundary conditions of FEM is the free surface and the triangular (in 2D) or tetraedric (in 3D) unstructured meshes are well adapted to complex media and topography. However, low polynomial basis are inadequate with fine spatial discretization and the required discretization to obtain

precise and non-dispersive solution is numerically costly.

Parallel, at the end of the 20th century, the Spectral Element Method (SEM), widely used in fluid dynamics (Patera, 1984; Korczak and Patera, 1986; Karniadakis, 1989), has been adapted to seismic wave propagation (Komatitsch et al., 1998; Komatitsch and Tromp, 1999; Komatitsch et al., 2005; Festa and Vilotte, 2005). The SEM is a variant of FEM based upon a high-order piecewise polynomial approximation of the weak formulation of the wave equation which leads to a spectral convergence ratio as the interpolation order increases.

In this method, the wave-field is represented in terms of high-degree Lagrange interpolants, and integrals are computed based upon Gauss-Lobatto-Legendre (gll) quadrature. This combination leading to a perfectly diagonal mass matrix leads in turn to a fully explicit time scheme which leads itself very well to numerical simulations on parallel computers.

SEM inherits the flexibility and the natural free surface condition of the FEM (Tromp et al., 2008). The typical element size that is required to generate an accurate mesh is of the order of λ, λ being the smallest wavelength of waves traveling in the model. Models are meshed with quadrangles (2D) and hexaedras (3D) using the open-source software package GMSH (Geuzaine and Remacle, 2009). It is particularly well suited to handle complex geometries and interface matching conditions (Cristini and Komatitsch, 2012). In order to simulate infinite or semi-infinite domain, SEM can use Perfect Match Layers boundary conditions (Bérenger, 1994; Festa and Vilotte, 2005) but are not used here.

Physical modeling: MUSC system

The MUSC system (Bretaudeau et al., 2008, 2011, 2013) is built to experimentally reproduce field seismic data with a great accuracy on reduces scale model. Figure 1 shows the bench and its components : it is composed of a honeycomb tab and two arms which control the source and the receiver position with a precision of 10 μm.

The receiving system of MUSC system is a laser interferometer based on a phase shift of the reflected laser signal due to the particular displacement at the surface of the model during the seismic waves propagation in the medium. A real-time calibration value enables a continuous conversion to a nanometric displacement. The focal diameter of the laser on the model surface is about several micrometers and allows a detection limit of 2.5 nm (few) in the frequency range from 20 kHz to 20 MHz. The laser interferometer constitutes a non coupled receiver which avoid the complicated modeling of the coupling effect on measurement.

But using a laser source needs more security protocols in the laboratory and up to now, the seismic source in the MUSC laboratory is simulated by a piezoelectric transducer linked to a launching and synchronization system. It allows to choose the source function, i.e., a waveform like a Gauss or Ricker function, the central frequency f_0 and the time delay t_0 . For that, the source is generated by a waveform generator and is then amplified before being transmitted to the small-scale-model.

For the purpose of reduced scale modeling, the change of scale must keep the relationship between observables, i.e. amplitudes and time arrivals. Concerning the amplitude, the quality factor Q will be chosen to be in the same range as the materials of near surface. For the time arrivals, the key parameter is the rate between the propagated seismic wavelength

and the spatial dimensions of the experience that includes the model geometry, the spatial increment between the sources and the receivers positions, but also the dimensions of the source impact. In the framework of seismic physical modeling, this latter must be as close as possible to a point source in order to simulate the spatial energy repartition of a weight drop at the soil surface, i.e. with an isotropic directivity of the emitted P waves.

In the MUSC system, the main frequency bands used for reduced scale data are [20 KHz ; 200 KHz] and [300 KHz; 800 KHz], respectively called here "low frequency band" and" high frequency band". For the lower spectral band, a commercial piezo-electric transducer is used without any coupling gel. For the higher band, the piezoelectric source is coupled through a conical adapter which is sticked to the transducer in order to obtain the expected impact surface. The resulting source pattern is isotropic enough in the spectral band of interest (see (Bretaudeau et al., 2011) for more details).

The lower frequency band is well adapted to simulate seismic experiment applied to near surface through the scales ratios proposed in tables 1 and 2. In the first case (table 1), a central frequency of 100 KHz in the laboratory corresponds to a central frequency of 100 Hz on the field, whereas in the second one (table 2) a central frequency of 100 KHz in the laboratory corresponds to a central frequency of 50 HZ on the field. Note that with these propositions, the quality factor Q and the density ρ are modeled with a ratio equal to 1, i.e. they remain the same at both of the scales. Actually small-scale models are generally made of thermoplastic or casting epoxy resin materials (Bretaudeau et al., 2013, 2011, 2008).The mechanical properties of these materials provide attenuation characteristics close to natural soil materials of subsurface media. Their seismic velocities are about 2 times of those in subsurface materials as proposed in table 2. The possibilities of combinations can generate the impedance contrasts encountered in the geophysical issues.

The MUSC bench presented above has been studied for simulating with a great repro-
ducibility the typical field campaigns of subsurface seismic measurement. The validation
was achieved by comparison between small scale measurement and numerical data (ref).
Results have shown a great reproducibility of the converted and diffracted events recorded
on the vertical component. The amplitudes analysis had been conducted through 2D-3D
corrections and small discrepancies remained due to the difficulty of taking into account
the S and P waves in the same way. For this reason, we propose here to refine the study by
testing a more recent correction methodology (ref) as well as providing experimental and
numerical, 2D and 3D data. This study will be achieved through data carried out on two
models that are presented below.

Reduced-scale models

distances are in mm (acquisition length around 50 mm typically) and time unit is ms.(
V_P, V_S etc...) The models are generally over-sized to easily separate reflected waves on
boundaries from the rest of the signal.

RESULTS

From point-source to line-source response

In the framework of wave propagation modeling and imaging methods, most of available
algorithms are limited to the two-dimensional approximation especially for computational
cost causes. More, a widely used way to validate imaging methods consists in inverse crime
while the validity of applications on real dataset is conditioned by strong *a priori* and a
weak knowledge of the target. All of these leads to a limited validation of the efficiency

9

imaging methods to recover parameter models. Thus, it is critical for 2D inversion of field date to accurately correct the geometrical spreading.

180　Point-source data can corrected from geometrical spreading using a simple two-steps signal processing: (1) convolving each trace by $\sqrt{t^{-1}}$, where t is the time, to correct the phase shift of $\pi/4$ (2) applying a taper $\sqrt{t}$ to all traces to correct amplitudes. Some variation exist, for examples, using a linear source wavelet estimation method to correct the phase (Bretaudeau et al., 2013) or applying an offset conditioning (Tran et al., 2013). To correct some

185　biases of these methods, Forbriger et al. (2014) and Schafer et al. (2014) have introduced, and successfully applied to synthetic data, the *hybrid method*. In the *hybrid method* the geometrical spreading correction is conditioned by: (1) the offset, (2) the knowledge of the wave propagation velocities in the medium and (3) a user defined ratio used to smoothly correct amplitudes from near to far offsets. The results are thus strongly dependent of

190　user's *a priori* and attempts. However, this kind of signal corrections are valid only for two-dimensional (x, z) medias invariant along the y-axis.

In other cases, 3D data are corrected or process *on the fly*, or used as is in algorithm using a 2.5D approximation.

Thus, the missing step between purely numerical validation and real data applications can

195　be the use of experimental line-source seismograms recorded under controlled conditions.

Here, we take advantage of the experimental framework to explore an alternative approach specific to MUSC system. Figure 3 presents a schematic representation of the principle for this kind of experiment. Theoretically, the stack of all receiver with the same offset will results in a pseudo line-source response. Yet, to simplify the experiment, an other

200　way is to consider only one receiver per offset, on a line perpendicular and centered to the

10

defined line-source. All traces of each common receiver gather are then stacked together to obtain the line-source response. In order to apply this protocol, we have to choose a line-source's length L sufficiently great to be assimilated to a cylindrical source and above all a suitable sampling interval Δs between each point-source constituting the pseudo line-source to ensure applicability of the *Huygen's principle*.

For this experiment, we choose an homogeneous block of *F50 pure* epoxy-resin (see table 1 for physical parameters) with dimensions $500 \times 504 \times 115$ mm ($x \times y \times z$). Given the material's properties, we choose $L = 240\ mm$ and $ds = 0.5\ mm$ which leads to 481 point-source locations. Four receiver positions have been selected: 45, 50, 55 and 60 mm offset perpendicular to the line-source. The source wavelet is a Ricker with a central frequency $f_0 = 100\ kHz$.Each receiver is perpendicular to and centered on the line-source. For each receiver position, all recorded traces are stacked together to obtain an equivalent two-dimensional line-source response.

We first apply this method using 2D and 3D numerical modeling for 3D point-source, 3D line-source and 2D cylindrical source with a complete acquisition of 120 receivers spaced of 1 mm and a minimum offset of 45 mm. For these experiments, we did not take into account the quality factor $\mathcal{Q}$. Figure 5a shows the comparison between point-source response (3D) and line-source response (2D). As expected, both amplitude and phase are differents. Then, we applied the *hybrid method* (**?**) on the point-source response to obtain the equivalent line-source response. Figure 5b shows that the *hybird method* is able to produce equivalent line-source response with a good agreement.

To evaluate the efficiency of the method, experimental line-source responses will be compared to point-source and equivalent line-source responses using the cross-correlation co-

efficient (**cc**) and the root mean square (**rms**) ratio. These values are presented in table 2. $\mathbf{cc}_init$ and $\mathbf{rms}_init$ correspond to direct evaluation whereas $\mathbf{cc}_final$ corresponds to the best **cc** obtained and $\mathbf{rms}_final$ is the corresponding **rms**.

We now apply this method to experimental data on the equivalent real reduced-scale model. Figures 6(a) show the comparison between experimental traces obtained using a point-source and a line-source for source-receiver offsets 50, 55, 60 and 65 mm respectively. It is straightforward that these waveforms are not similar in terms of both phases (**cc**<0.75) and amplitude (**rms**>0.4). Even after amplitude fitting, point-source response to the line-response in term of phase (**cc**<0.8), amplitudes do not match (**rms**>0.4). These results confirm that using raw point-source responses in a two-dimensional inversion process or imaging method can be critical in terms of convergence and validity of the results since these methods are built over phase and/or amplitude similarity.

Figures 6(b) show the comparison between experimental traces using a line-source and a point-source after geometrical spreading corrections (equivalent line-source response) using the same parameters than for numerical experiment. The cross-correlation coefficient **cc** for these waveforms are greater than 0.95 and rms<0.25. These results denote that the experimental line-source response is correct in terms of phase compared to an equivalent line-source response. However, **rms** are quite great even if they are smaller than previously. This can be explained by small differences in terms of waveforms and phases which are critical in the final **rms** results. Moreover, the *hybrid* method to obtain the equivalent line-source response from a point-source response needs accurate parametrization to obtain the best result which is not necessarily in a good agreement with the attempt true line-source response.

These results show that the line-source emulation on the MUSC system is efficient and can produce data suitable for imaging methods such as 2D FWI.

Experimental source reproducibility

We have shown the MUSC system is able to generate high quality 2D experimental seismograms. However, experimental data, as other, must be reproducible to be used as a reference or in an inversion process. As shown by Bretaudeau et al. (2011), the source waveform injected in the reduced-scale model by the piezo-electric source is not similar to the selected theoritical one. Figure (?), of data recorded in an homogeneous model, shows clearly multiple wavefront following the main arrival. After Bretaudeau et al. (2011), these multiples are generated inside the conical adapter of the piezo-electric source.

To assess the ability of MUSC system to provide reproducible data, *i.e.* to evaluate the reproducibility of the source impact, several physical modeling were performed on the same homogeneous epoxy-resin block as in previous section.

Ten realizations have been acquired on this model with a similar geometry setup, i.e. 120 receivers positions with an increment equal to 1 mm and a minimum offset of 10 mm. The numerical wavelet sent to the piezoelectric transducer source is a Ricker signal with a central frequency of 100 kHz. However, the source waveform is modified by the physical coupling effect of the transducer.

A mean shot gather, calculated from the ten experiments, is used as reference seismogram. Figure 8 shows the central trace of each realization and **cc** gives the correlation coefficient of each trace with the reference one. The **cc** are always greater than 0.98 which demonstrate the very high reproducibility of data generated by the MUSC system.

13

In a second step, a unique source wavelet is estimated using a linear source wavelet estimation method based on a stabilized deconvolution (Pratt, 1999). The source wavelet estimation takes into account the ten experiments together and allows to obtain a mean effective source suitable for each experiment. The resulting source wavelet is applied to the synthetic signals (figure 10). The corrected seismograms are in good agreement with the experimental seismograms (correlation coefficients > 0.96) confirms the great efficiency of the wavelet source assessment process.

These last results, based on an average estimated source wavelet show that the effective impulse source emitted by the transducer in the MUSC system measurement bench is stable enough to ensure a robust reproducibility of the source. Therefore, concerning the key issue of the source knowledge, experimental data acquired in the MUSC system can be efficiently processed by imaging methods like Full Waveform Inversion (FWI) with only one estimation step for all the multi-source and multi-receivers data.

However, this last result does not mean that the source will be the same for an experiment for an other experiment on an other model. Thus, we consider now a more complex model, called *BiAlt*. This model , shown in figure (???) is a two-layer model with a central alteration. We generate synthetic seismogram with the 2D SEM algorithm and using the mean effective source wavelet estimated on homogeneous block as a source function. Figure 12 shows that the synthetic seismogram using the effective source wavelet is in good agreement with the experimental one...

This last result shows that the MUSC source is stable from an experiment to an other and can be consequently injected as an input in modeling and imaging methods without any pre-processing or *on the fly* source inversion.

CONCLUSIONS

These two studies allow to refine the capacity of the physical modeling designed for seismic experiments simulation by 1) completing the validation of the measurement through comparison of numerical and experimental data generated by a realistic 2D source line and 2) assessing the reproductivity of the effective source emitted in a model. These improvements allow to provide and distribute experimental reduced scale data to the scientific community as benchmark datasets.

PLOTS

Equations

Figures
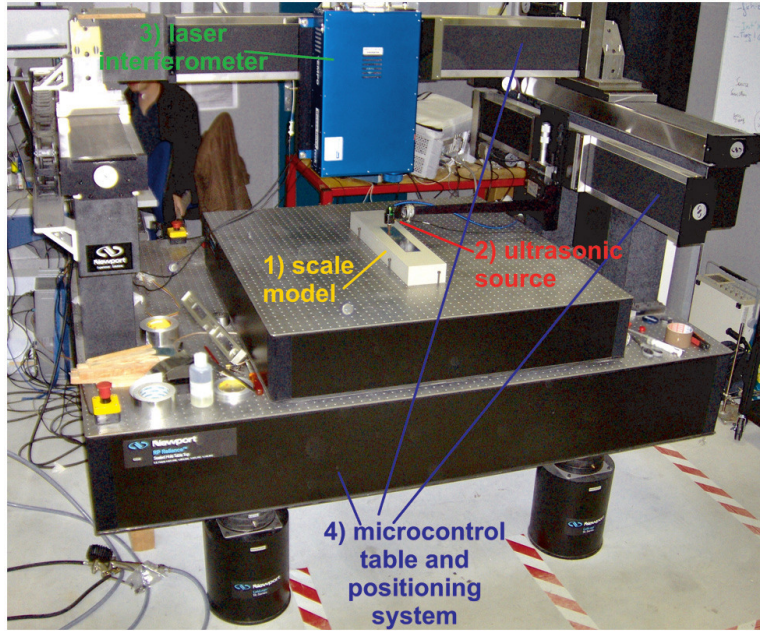
Figure 1: Photograph of the MUSC ultrasonic laboratory (from Bretaudeau et al. (2013))with its four components: (1) a small-scale model of the underground, (2) an optical table with two automated arms moving above the model, (3) a laser interferometer recording ultrasonic wave propagation at the model surface, and (4) a piezoelectric ultrasonic source generating ultrasonic waves in the model.
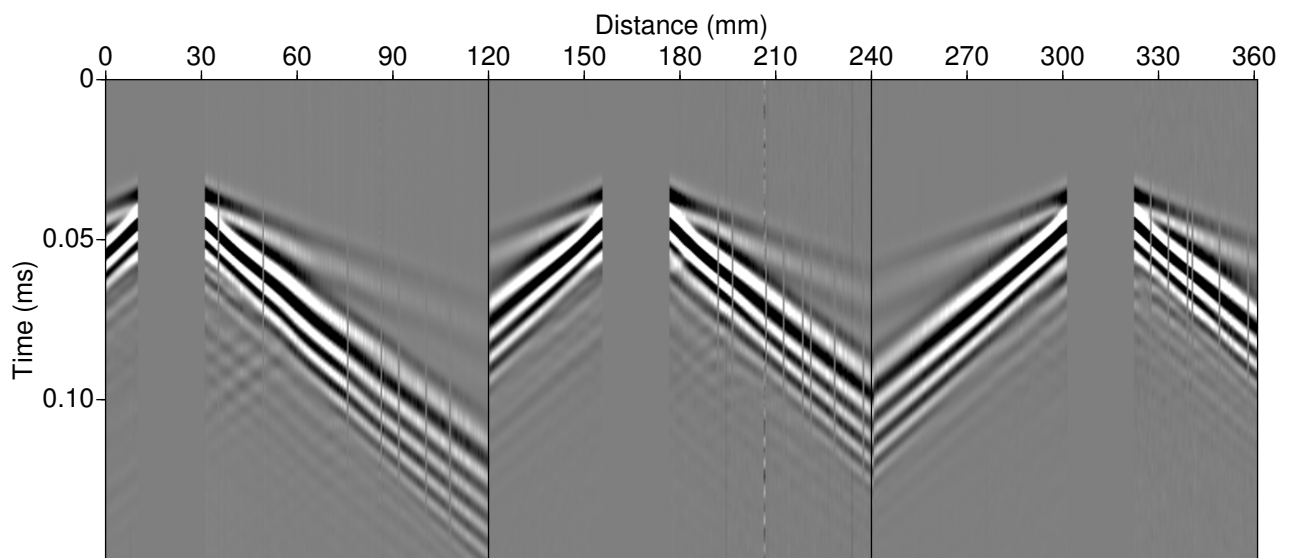
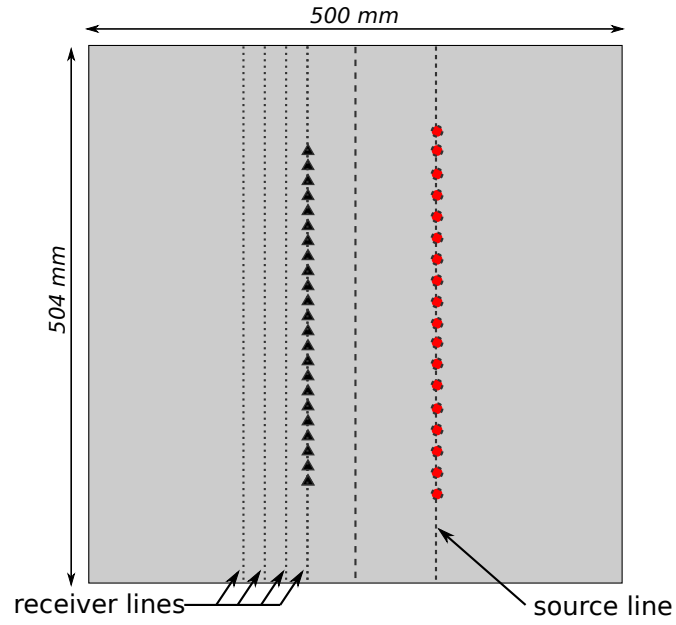Figure 2: Example of multi-source multi-receiver record on the MUSC system for a two-layer model (bialt).

Figure 3: Schematic representation of the acquisition geometry used to generate experimental line-source, *i.e.* an equivalent of cylindrical source use in two-dimensional modeling. Black traingle and red circle represent receivers and sources, respectively.
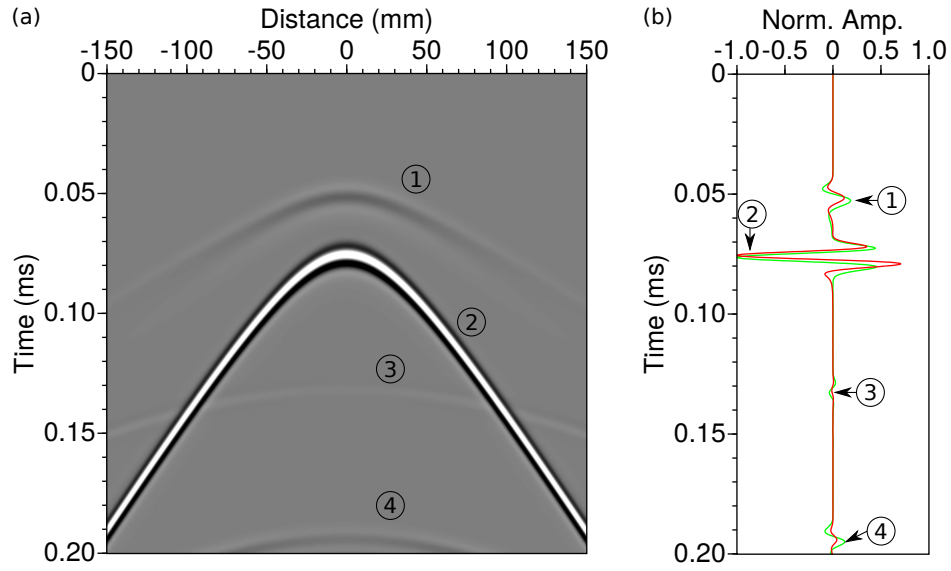
Figure 4: (a) Resulting seismogram at one receiver position for the experimental line-source. (b) Comparison between point-source response in red (central trace of (a)) and line-source response in green (stack of (a)). Some wavefront are pointed: (1) P-wave, (2) surface wave, (3) reflected PP and (4) reflected PSv -wave on the bottom of the model.
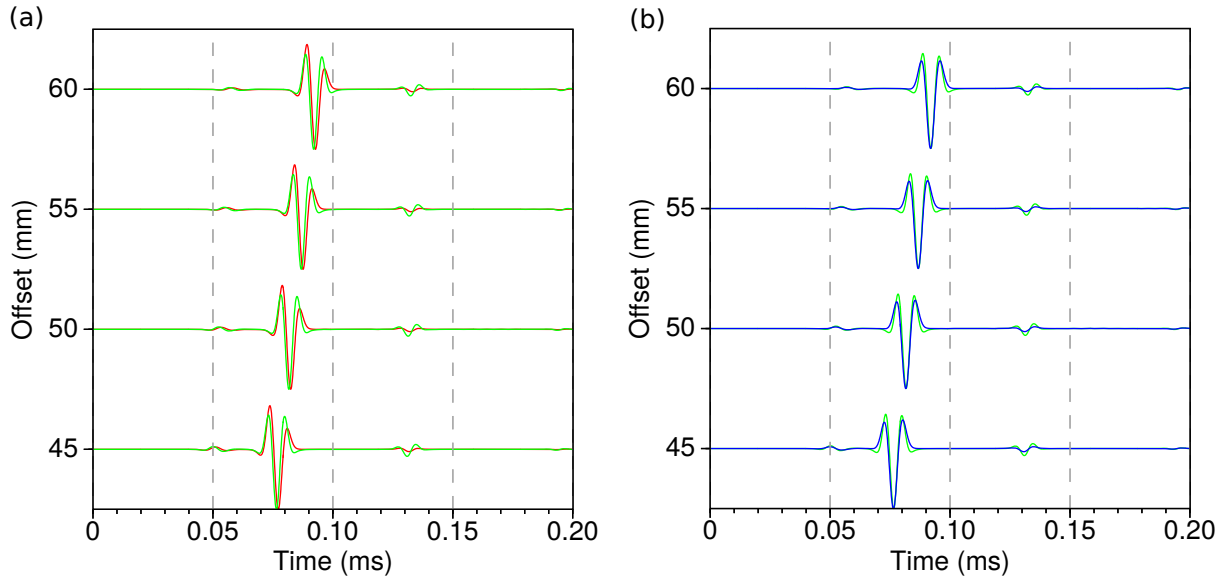
Figure 5: (a) Comparison between synthetic seismograms for a point-source (red) and for a line source (green), for 45, 50, 55 and 60 mm source-receiver offsets respectively. (b) Comparison between synthetic seismograms for a line-source (green), and a point-source response corrected from geometrical spreading (blue) for same source-receiver offsets as (a).
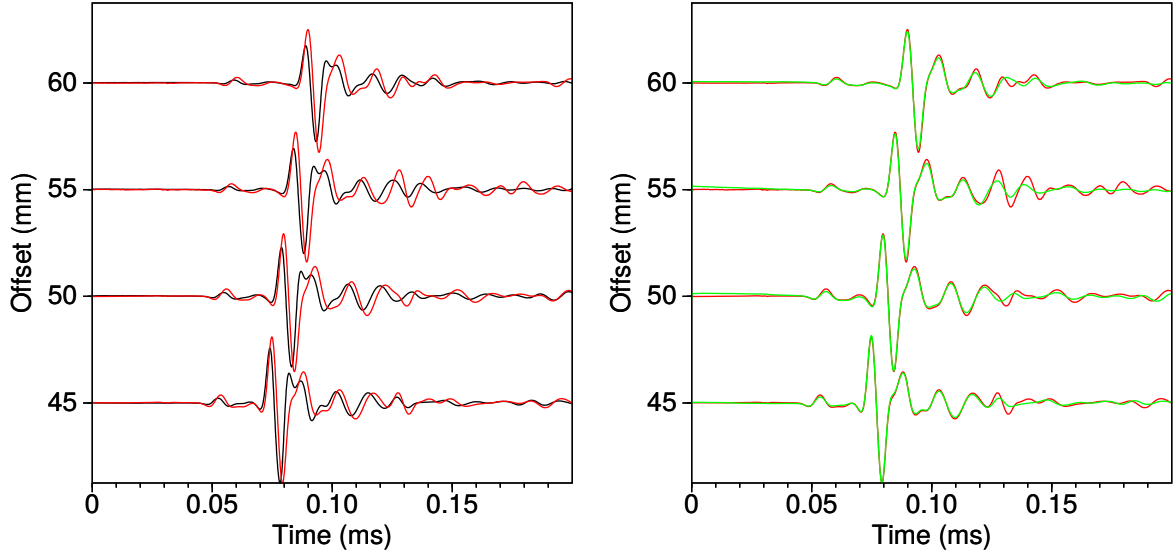
Figure 6: (a) Comparison between experimental seismograms for a point-source (red) and for a line source (black), for 45, 50, 55 and 60 mm source-receiver offsets respectively. (b) Comparison between experimental seismograms for a line-source (black), and a point-source response corrected from geometrical spreading (green) for same source-receiver offsets as (a).
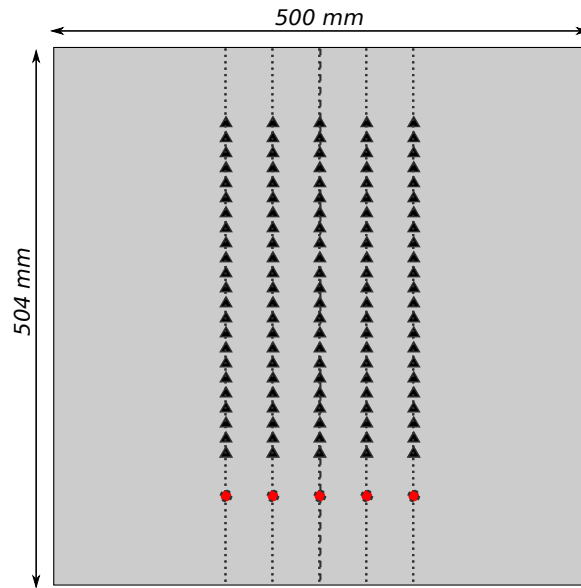
Figure 7: Schematic representation of the acquisition geometry used to assess the data reproducibility using the MUSC system. Black traingle and red circle represent receivers and sources, respectively.
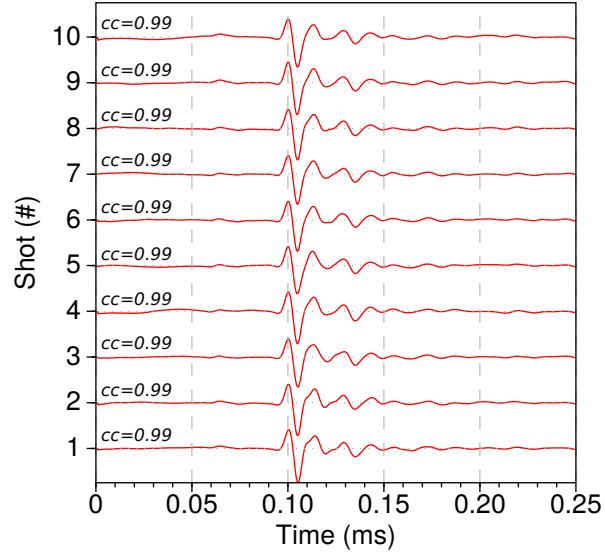
Figure 8: Central trace for each of the ten analogic experiment. **cc** gives the correlation factor of each central trace with respect to a mean trace.
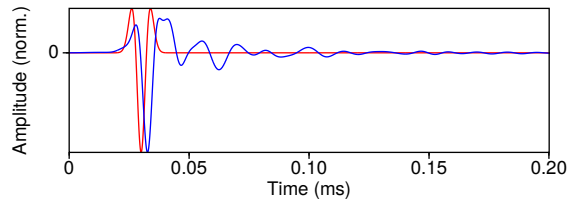

Figure 9: Comparison between the theoritical Ricker source send to the transducer and the effective source wavelet injected in the model.
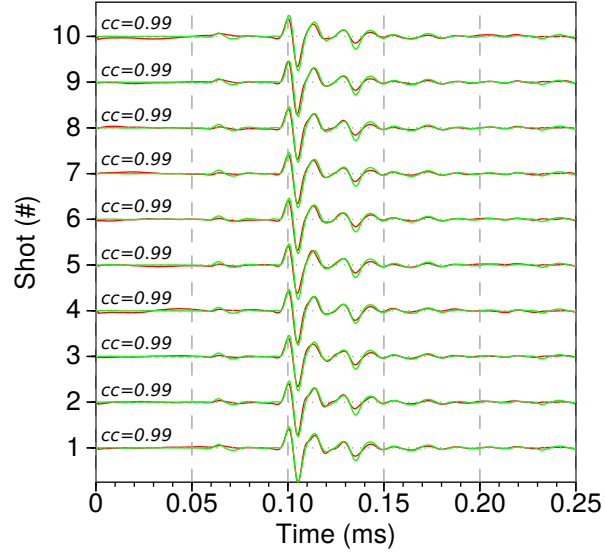
Figure 10: Comparison between analogic central traces (grey) and numerical traces corrected from the estimated effective source (black) for each experiment. **cc** gives the correlation coefficient.
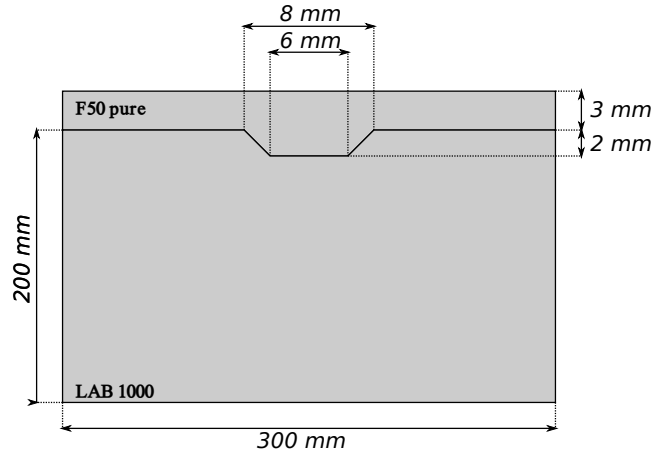

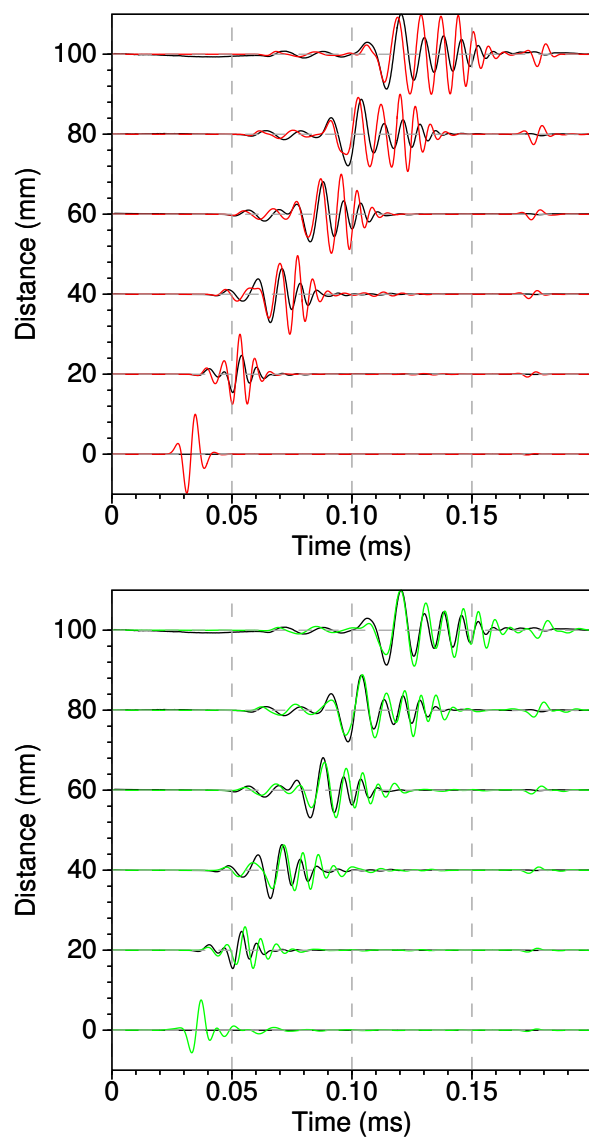Figure 11: Schematic representation of the so-called *BiAlt* model.

24

Figure 12: .

300 **Tables**

material	V_P (m/s)	V_S (m/s)	V_R (m/s)	ρ (kg/m^3)	Q
Aluminium	5630	3225	–	2700	–
F50 pure	2300	1030	965	1300	30
F50 200%	2820	1425	1328	1766	–
F50 240%	2968	1496	1388	1822	–
LAB1000	2850	1400	1310	1500	75

Table 1: Physical properties of some materials used to build small scale models. V_P, V_S and V_R are the P-wave velocity, S-wave and the Rayleigh wave velocity, respectively. ρ is the density and Q is the quality factor.

	90 mm	95 mm	100 mm	105 mm
$cc1_{init}$	0.702	0.725	0.728	0.728
$rms1_{init}$	0.794	0.760	0.762	0.774
$cc1_{final}$	0.940	0.953	0.951	0.949
$rms1_{final}$	0.358	0.317	0.325	0.343
$cc2_{init}$	0.954	0.987	0.988	0.988
$rms2_{init}$	0.304	0.162	0.155	0.154
$cc2_{final}$	–	–	–	–
$rms2_{final}$	–	–	–	–

Table 2: .

ACKNOWLEDGMENTS

REFERENCES

Bérenger, J. P., 1994, A perfectly matched layer for the absorption of electromagnetic waves: Journal of Computational Physics, **114**, 185–200.

Berkhout, A., D. Verschuur, and G. Blacquiere, 2012, Illumination properties and imaging promises of blended, multiple-scattering seismic data: a tutorial: Geophysical Prospecting, **60**, 713–732.

Bishop, T., K. Bube, R. Cutler, R. Langan, P. Love, J. Resnick, R. Shuey, and D. Spinder, 1985, Tomographic determination of velocity and depth in laterally varying media: Geophysics, **50**, 903–923.

Bohm, G., J. M. Carcione, D. Gei, S. Picotti, and A. Michelini, 2015, Cross-well seismic and electromagnetic tomography for co 2 detection and monitoring in a saline aquifer: Journal of Petroleum Science and Engineering, **133**, 245–257.

Bretaudeau, F., R. Brossier, D. Leparoux, O. Abraham, and J. Virieux, 2013, 2d elastic full-waveform imaging of the near-surface: application to synthetic and physical modelling data sets: Near Surface Geophysics.

Bretaudeau, F., D. Leparoux, and O. Abraham, 2008, Small scale adaptation of the seismic full waveform inversion method - application to civil engineering applications.: The Journal of the Acoustical Society of America, **123**.

Bretaudeau, F., D. Leparoux, O. Durand, and O. Abraham, 2011, Small-scale modeling of onshore seismic experiment: A tool to validate numerical modeling and seismic imaging methods: Geophysics, **76(5)**, T101–T112.

Cristini, P., and D. Komatitsch, 2012, Some illustrative examples of the use of the spectral-element method in ocean acoustics.: Journal of the Acoustical Society of America.

Favretto-Cristini, N., A. Tantserva, P. Cristini, B. Ursin, D. Komatitsch, and A. Aizen-

berg, 2013, Numerical modeling of zero-offset laboratory data in a strong topographic

environment: results for a spectral-element method and a discretized kirchhoff integral method: Earthquake Science.

Festa, G., and J. Vilotte, 2005, The Newmark as velocity-stress time-staggering: an efficient PML implementation for spectral element ssimulation of elastodynamics: Geophysical Journal International, **161**, 798–812.

Forbriger, T., L. Gross, and M. Schafer, 2014, Line-source simulation for shallow-seismic data. part 1: theoretical background: Geophysical Journal International, **198**, 1387–1404.

French, W. S., 1974, Two-dimensional and three-dimensional migration of model-experiment reflection profiles: Geophysics, **39(3)**, 265–277.

Geuzaine, C., and J. Remacle, 2009, Gmsh: a three-dimensional finite element mesh generator with built-in pre- and post-processing facilities.: International Journal for Numerical Methods in Engineering, **79**, 1309–1331.

Guofeng, L., L. Yaning, R. Li, and M. Xiaohong, 2013, 3d seismic reverse time migration on gpgpu: Computers & Geosciences, **59**, 10–23.

Hilterman, F., 1970, Three-dimensional seismic modeling: Geophysics, **35**, 1020–1037.

Howes, E., L. Tejada-Flores, and L. Randolph, 1953, Seismic model study: Journal of the Acoustical Society of America, **25**, 915–921.

Hulbert, G. M., and T. J. Hughes, 1990, Space-time finite element methods for second-order hyperbolic equations: Computer Methods in Applied Mechanics and Engineering, **84**, 327–348.

Isaac, J. H., and D. C. Lawton, 1999, Image mispositioning due to dipping ti media: A physical seismic modeling study: Geophysics, **64**, 1230–1238.

Karniadakis, G. E., 1989, Spectral element simulations of laminar and turbulent flows in

complex geometries: Applied Numerical Mathematics, **6**, 85 – 105. (Special Issue on Spectral Multi-Domain Methods).

350   Komatitsch, D., and J. Tromp, 1999, Introduction to the spectral-element method for three-dimensional seismic wave propagation: Geophysical Journal International, **139**, 806–822.

Komatitsch, D., S. Tsuboi, and J. Tromp, 2005, The spectral-element method in seismology.

Komatitsch, D., J. P. Vilotte, R. Vai, J. M. Castillo-Covarrubias, and F. J. Sánchez-Sesma, 1998, The Spectral Element Method for Elastic Wave Equation: Application to 2-D and

355   3-D Seismic Problems: International Journal for Numerical Methods in Engineering, **45**, 1139–1164.

Korczak, K. Z., and A. T. Patera, 1986, An isoparametric spectral element method for solution of the navier-stokes equations in complex geometry: Journal of Computational Physics, **62**, 361 – 382.

360   Levander, A., 1988, Fourth-order finite-difference p-sv seismograms: Geophysics, **53**, 1425–1436.

Lysmer, J., and L. A. Drake, 1972, A finite element method for seismology: Methods in computational physics, **11**, 181–216.

Moczo, P., J. Kristek, and L. Halada, 2004, The finite-differences method for seismologists:

365   An introduction: Comenius University, Bratislava.

Morozov, I., 2004, Crustal scattering and some artefacts in receiver function images: Bulletin of the Seismological Society of America, **94**, 1492–1499.

Patera, A. T., 1984, A spectral element method for fluid dynamics: Laminar flow in a channel expansion: Journal of Computational Physics, **54**, 468–488.

370   Perez Solano, C., D. Donno, and H. Chauris, 2014, Alternative waveform inversion for surface wave analysis in 2-d media: Geophysical Journal International, **198**, 1359–1372.

Pratt, R. G., 1990, Frequency domain elastic wave modeling by finite differences: A tool for cross-hole seismic imaging.: Geophysics, **55**, 626–632.

———, 1999, Seismic waveform inversion in the frequency domain, Part 1: Theory and verification in a physical scale model: Geophysics, **64**, 888–901.

Rieber, F., 1936, Visual presentation of elastic wave patterns under various structural conditions: Geophysics, **1**, 196–218.

Robertsson, J., J. Blanch, and W. Symes, 1994, Viscoelastic finite-difference modeling.: Geophysics, **59**, 1444–1456.

Saenger, E. H., and T. Bohlen, 2004, Finite-difference modeling of viscoelastic and anisotropic wave propagation using the rotated staggered grid: Geophysics, **69**, 583–591.

Saenger, E. H., N. Gold, and A. Shapiro, 2000, Modeling the propagation of elastic waves using a modified finite-difference grid: Wave Motion, **31**, 77–92.

Sarkar, D., A. Bakulin, and R. L. Kranz, 2003, Anisotropic inversion of seismic data for stressed media: Theory and a physical modeling study on berea sandstone: Geophysics, **68**, 1–15.

Schafer, M., L. Gross, T. Forbriger, and T. Bohlen, 2014, Line-source simulation for shallow-seismic data. part2: full-waveform inversion – a synthetic 2-d case study: Geophysical Journal International, **198**, 1405–1418.

Seron, F. J., F. J. Sanz, M. Kindelan, and J. I. Badal, 1990, Finite-element method for elastic wave propagation: Communications in applied numerical methods, **6**, 359–368.

Stekl, I., and R. G. Pratt, 1998, Accurate visco-elastic modeling by frequency-domain finite differences, using rotated operators.: Geophysics, **63**, 1779–1794.

Tran, K. T., M. McVay, M. Faraone, and D. Horhota, 2013, Sinkhole detection using 2d full seismic waveform tomography: Geophysics, **78**, R175–R183.

32

Tromp, J., D. Komatitsch, and Q. Liu, 2008, Spectral-element and adjoint methods in seismology.: Commun Comput Phys.

Virieux, J., 1986, P-sv wave propagation in heterogeneous media: velocity-stress finite-difference method: Geophysics, **51**, 889–901.

Virieux, J., and S. Operto, 2009, An overview of full-waveform inversion in exploration geophysics: Geophysics, **74**, WCC1WCC26.

Wirgin, A., 2004, The inverse crime: ArXiv Mathematical Physics e-prints. (Provided by the SAO/NASA Astrophysics Data System).

Wong, J., K. W. Hall, E. V. Gallant, R. Maier, M. Bertram, and D. C. Lawton, 2009, Seismic physical modeling at university of calgary: CSEG recorder, **34**.